Version 4
May 7, 2015

Studies of the diffractive photoproduction of isolated photons at HERA

ZEUS Collaboration

Abstract

In this analysis using the ZEUS detector at HERA, the photoproduction of isolated photons is measured in diffractive events. Cross sections are evaluated in the photon transverse-energy and pseudorapidity ranges $5 < E_T^{\gamma} < 15$ GeV and $-0.7 < \eta^{\gamma} < 0.9$, inclusively and with a jet with transverse-energy and pseudorapidity in the ranges ranges $4 < E_T^{\text{jet}} < 35$ GeV and $-1.5 < \eta^{\text{jet}} < 1.8$, for an integrated luminosity of 374 pb^{-1}. Further kinematic variables studied include the fractions of the incoming photon energy and of the colourless exchange ("Pomeron") energy that are imparted to a photon-jet final state,
. Comparison is made to predictions from the Rapgap Monte Carlo simulation.

1 Introduction

In a distinctive class of hadronic particle interactions, known as diffractive, one or more incoming hadrons scatter in such a way that a colour-neutral object is exchanged. This object, frequently referred to as the “pomeron”, is believed to consist to a large extent of gluons. Diffractive scattering off protons may be initiated by a second incoming hadron, or even by a real or virtual photon. At the HERA *ep* collider, diffractive processes have been studied both in photoproduction and in deep inelastic scattering, the photoproduction processes consisting of those in which the exchanged virtual photon is quasi-real. A commonly measured final state consists of two hadronic jets. The hard diffractive process is characterised by a forward nucleon, which requires specialised equipment for its measurement, followed by a “gap” in rapidity in which little or no energetic scattering is found until the central region of the process where the hard final state is detected and measured.

Following several studies of diffractive dijets in photoproduction at HERA [13–15], the present paper gives measurements in which a hard isolated “prompt” photon is detected in the central region of the ZEUS detector and may be accompanied by a jet. Such processes, while rare, are interesting for several reasons. An outgoing photon must be radiated from a charged partonic object, namely a quark, and therefore demonstrates the presence of a quark content in the pomeron or of higher-order processes in which both the pomeron and incident photon couple to quarks. Specific models of the hard diffractive process may be tested.

The observed processes also include “fragmentation processes” in which a photon is radiated within a jet. Such processes are suppressed by requiring that the outgoing photon be isolated.

The present measurements follow an earlier study by H1 [16] of inclusive diffractive high energy prompt photons as a function of transverse momentum. Analyses of isolated photons in non-diffractive photoproduction have also been made by the ZEUS and H1 collaborations [2–7], as well as in deep inelastic scattering (DIS) [8–11].

2 Kinematic quantities

In “direct” photoproduction processes, the entire incoming photon is absorbed by an outgoing quark from the incoming proton, while in “resolved” processes, the photon’s hadronic structure provides a quark or gluon that interacts with a parton from the proton. These two classes of process, which are unambiguously defined only at lowest order, may be partially distinguished in events containing a high-E_T photon and a jet by means of the quantity

$$x_\gamma^{\text{meas}} = \frac{E^\gamma + E^{\text{jet}} - p_Z^\gamma - p_Z^{\text{jet}}}{E^{\text{all}} - p_Z^{\text{all}}}, \tag{1}$$

which measures the fraction of the incoming photon energy that is given to the photon and the jet. The quantities E^γ and E^{jet} denote the energies of the photon and the jet, respectively, p_Z denotes the corresponding longitudinal momenta[1], and the suffix "all" refers to all the final-state particles or detector-measured objects in an event. These sums do not include the outgoing proton and its excitation products, if any, which emerge unmeasured close to the proton beam direction. At LO, $x_\gamma^{\text{meas}} = 1$ for direct events, while resolved events can generate any value in the range (0,1). At higher order, the first statement no longer precisely holds, but the presence of direct processes generates a prominent peak in the cross section at high x_γ^{meas}.

When the proton radiates an object such as a pomeron, which interacts with all or part of an incoming photon, the fraction of the proton energy taken by the radiated pomeron is given to a good approximation by:

$$x_{I\!P} = (E^{\text{all}} + p_Z^{\text{all}})/2E_p, \tag{2}$$

where E_p is the energy of the proton beam.

The fraction of the pomeron energy that takes part in the hard interaction that generates the outgoing photon and jet is given to a good approximation by: [15]

$$z_{I\!P}^{\text{meas}} = \frac{E^\gamma + E^{\text{jet}} + p_Z^\gamma + p_Z^{\text{jet}}}{E^{\text{all}} + p_Z^{\text{all}}}, \tag{3}$$

where the sum is as before. The alternative formulation

$$z_{I\!P}^{\text{obs}} = (E_T^\gamma \exp \eta^\gamma + E_T^{\text{jet}} \exp \eta^{\text{jet}})/(E^{\text{all}} + p_Z^{\text{all}}),$$

where E_T denotes transverse energy, yields equivalent results.

3 Experimental set-up

The measurements are based on two data samples corresponding an integrated luminosities of 91 and 374 pb^{-1}, taken during the years 1998-200 and 2004-2007 respectively with

---

[1] The ZEUS coordinate system is a right-handed Cartesian system, with the Z axis pointing in the nominal proton beam direction, referred to as the "forward direction", and the X axis pointing towards the centre of HERA. The coordinate origin is at the centre of the central tracking detector. The pseudorapidity is defined as $\eta = -\ln\left(\tan\frac{\theta}{2}\right)$, where the polar angle, θ, is measured with respect to the Z axis.

the ZEUS detector at HERA. These are referred to as HERA-I and HERA-II samples respectively. During these periods, HERA ran with an electron or positron beam energy of 27.5 GeV and a proton beam energy of $E_p = 920\,\text{GeV}$. The samples include e^+p and e^-p data[2].

A detailed description of the ZEUS detector can be found elsewhere [17]. Charged particles were measured in the central tracking detector (CTD) [18] and a silicon micro vertex detector (MVD) [19] which operated in a magnetic field of 1.43 T provided by a thin superconducting solenoid. The high-resolution uranium–scintillator calorimeter (CAL) [20] consisted of three parts: the forward (FCAL), the barrel (BCAL) and the rear (RCAL) calorimeters. The BCAL covered the pseudorapidity range −0.74 to 1.01 as seen from the nominal interaction point, and the FCAL and RCAL extended the coverage to the range −3.5 to 4.0. Each part of the CAL was subdivided into elements referred to as cells. The barrel electromagnetic calorimeter (BEMC) cells had a pointing geometry aimed at the nominal interaction point, with a cross section approximately $5 \times 20\,\text{cm}^2$, with the finer granularity in the Z direction and the coarser in the (X, Y) plane. This fine granularity allows the use of shower-shape distributions to distinguish isolated photons from the products of neutral meson decays such as $\pi^0 \to \gamma\gamma$. The CAL energy resolution, as measured under test-beam conditions, was $\sigma(E)/E = 0.18/\sqrt{E}$ for electrons and $0.35/\sqrt{E}$ for hadrons, where E is in GeV.

The luminosity was measured [21] using the Bethe–Heitler reaction $ep \to e\gamma p$ by a luminosity detector which consisted of two independent systems: a lead–scintillator calorimeter [22] and a magnetic spectrometer [23].

4 Monte Carlo event simulation

Monte Carlo (MC) event samples were employed in the same way as previously [1] to evaluate the detector acceptance and event-reconstruction efficiency, and to provide signal and background distributions.

The program RAPGAP 3.2 was used to generate the diffractive process $pe \to pe\gamma X + \text{jet}$ for direct and resolved incoming virtual photon exchange, where X denotes the presence of hadronic remnants. The diffractive proton pdf set H1-B (2006) was used, and for the resolved photon the pdf set SaSG 1D LO.

The program PYTHIA 6.416 [27] was used to generate direct and resolved prompt-photon photoproduction processes for background calculations, and also $2 \to 2$ parton-parton scattering processes not involving photons ("dijet events"), making use of the CTEQ4 [28]

---

[2] Hereafter "electron" refers to both electrons and positrons unless otherwise stated.

and GRV [29] proton and photon parton densities. The program was run using the default parameters with minor modifications[3].

The isolated photons measured here are accompanied by backgrounds that arise from neutral mesons in hadronic jets, in particular π^0 and η, where the meson decay products create an energy cluster in the BCAL that passes the selection criteria for a photon. Although not generated diffractively, the dijet event samples enabled such background events to be extracted for use in the analysis.

Non-diffractive photoproduction event samples were also generated using the HERWIG 6.510 program [30], again with minor modifications to the default parameters. The PYTHIA and HERWIG programs differ significantly in their treatment of parton showers, and in the use of a string-based hadronisation scheme in PYTHIA but a cluster-based scheme in HERWIG.

The generated MC events were passed through the ZEUS detector and trigger simulation programs based on GEANT 3.21 [31]. They were then reconstructed and analysed using the same programs as used for the data.

5 Event selection and reconstruction

The basic event selection and reconstruction was performed as previously [1]. A three-level trigger system was used to select events online [17, 32, 33]:

- the first-level trigger required a loosely measured track in the CTD and a minimum energy deposited in the CAL;
- at the second level, the event conditions were tightened;
- at the third level, the event was reconstructed and a high-energy photon candidate was required. Most deep inelastic scattering events were rejected.

In the offline event analysis, some general conditions were applied as follows:

- to reduce background from non-*ep* collisions, events were required to have a reconstructed vertex position, $Z_{\rm vtx}$, within the range $|Z_{\rm vtx}| < 40\,{\rm cm}$;
- no scattered beam electron was permitted in the ZEUS detector;
- the accepted range of incoming virtual photon energies was defined by the requirement $0.2 < y_{\rm JB} < 0.7$, where $y_{\rm JB} = \sum_i E_i(1-\cos\theta_i)/2E_e$ and E_e is the energy of the electron beam. Here, E_i is the energy of the i-th CAL cell, θ_i is its polar angle and the sum

---

[3] In particular, the PYTHIA parameter PARP(67) was set to 4.0 and multiple parton interactions were turned off. In HERWIG the parameters ISPAC, QSPAC, and PTRMS were set to 2, 4.0, and 0.44.

runs over all cells [34]. The lower cut strengthened the trigger requirements and the upper cut further suppressed remaining deep inelastic scattering events.

The subsequent event analysis made use of energy-flow objects (EFO's) [35], which were constructed from clusters of calorimeter cells, associated with tracks when appropriate. Tracks not associated with calorimeter clusters were also included. Photon candidates were identified as EFO's with no associated track, and with at least 90% of the reconstructed energy measured in the BEMC. Those EFO's with wider electromagnetic showers than are typical for a single photon were accepted to make possible the evaluation of backgrounds. The photon energy scale was calibrated by means of an analysis of Deeply Virtual Compton Scattering events recorded by ZEUS, in which the detected final-state particles comprised a scattered electron, whose energy measurement is well understood, and a balancing outgoing photon.

Jet reconstruction was performed, making use of all the EFO's in the event including photon candidates, by means of the k_T clustering algorithm [36] in the E-scheme in the longitudinally invariant inclusive mode [37] with the radius parameter set to 1.0. By construction, one of the jets found by this procedure corresponds to or includes the photon candidate. An additional accompanying jet was required; if more than one was found, that with the highest transverse energy, $E_T^{\rm jet}$, was used. In the kinematic region used, the resolution of the jet transverse energy was about 15–20%, estimated using MC simulations.

To reduce the fragmentation contribution and the background from the decay of neutral mesons within jets, the photon candidate was required to be isolated from other hadronic activity. This was imposed by requiring that the photon-candidate EFO had at least 90% of the total energy of the reconstructed jet of which it formed a part. High-E_T photons radiated from scattered leptons were further suppressed by rejecting photons with a nearby track. This was achieved by demanding $\Delta R > 0.2$, where $\Delta R = \sqrt{(\Delta\phi)^2 + (\Delta\eta)^2}$ is the distance to the nearest reconstructed track with momentum greater than 250 MeV in the $\eta - \phi$ plane, where ϕ is the azimuthal angle. This latter condition was applied only at the detector level, and not in the hadron- or parton-level calculations.

Events were finally selected with the following kinematic conditions:

- each event was required to contain a photon candidate with a reconstructed transverse energy, E_T^γ, in the range $5 < E_T^\gamma < 15$ GeV and with pseudorapidity, η^γ, in the range $-0.7 < \eta^\gamma < 0.9$;
- The hadronic jet, when used, was required to have $E_T^{\rm jet}$ between 4 and 35 GeV and to lie within the pseudorapidity, $\eta^{\rm jet}$, range $-1.5 < \eta^{\rm jet} < 1.8$;
- to select diffractive events further conditions were applied, the first of which was that the maximum pseudorapdity for EFO's with energy above 0.4 GeV satisfied $\eta_{\rm max} < 2.5$;

- a second diffractive condition was that $x_{I\!P} < 0.03$;
- for the HERA-I data sample, the energy in the Forward Proton Calorimeter was required to be less than 1 GeV. This calorimeter was not present in the HERA-II running.

6 Extraction of the photon signal

The HERA-II data sample was used in the main analysis described here. The HERA-I data were analysed similarly, with the addition of the selection on the Forward Proton Calorimeter, and were used to provide a correction as described below.

The selected samples contain a substantial admixture of background events in which one or more neutral mesons, such as π^0 and η, have decayed to photons, thereby producing a photon candidate in the BEMC. The photon signal was extracted statistically following the approach used in previous ZEUS analyses [1,8–11]. The method made use of the energy-weighted width, measured in the Z direction, of the BEMC energy-cluster comprising the photon candidate. This width was calculated as

$$\langle \delta Z \rangle = \sum_i E_i |Z_i - Z_{\text{cluster}}| \, / \, (w_{\text{cell}} \sum_i E_i),$$

where Z_i is the Z position of the centre of the i-th cell, Z_{cluster} is the energy-weighted centroid of the EFO cluster, w_{cell} is the width of the cell in the Z direction, and E_i is the energy recorded in the cell. The sum runs over all BEMC cells in the EFO.

A further background arises from Deeply Virtual Compton Scattering events, characterised by an isolated photon accompanied by a "jet" that consists of a single electron. If the jet accompanying a photon candidate had just one charged track that was associated with an electromagnetic signal in the calorimeter, the event was removed from the sample.

The number of isolated-photon events in the data was determined by a χ^2 fit to the $\langle \delta Z \rangle$ distribution in the range $0.05 < \langle \delta Z \rangle < 0.8$, varying the relative fractions of the signal and background components as represented by histogram templates obtained from the MC. The fit was performed for each measured cross-section bin, with χ^2 values of typically XX per degree of freedom , verifying that the signal and background were well understood. Starting from selected samples of 867 (670) events without (with) a jet, the fit generated 433±33 (369±30) photon events.

A bin-by-bin correction method was used to determine the production cross section in a given variable, by means of the relationship

$$\frac{d\sigma}{dY} = \frac{\mathcal{A}\, N(\gamma)}{\mathcal{L}\, \Delta Y}, \tag{4}$$

where $N(\gamma)$ is the number of photons in a bin as extracted from the fit, ΔY is the bin width, $\mathcal{L}$ is the total integrated luminosity, and $\mathcal{A}$ is the acceptance correction. The acceptance correction was calculated, using MC samples, as the ratio of the number of events that were generated in the given bin to the number of events obtained in the bin after event reconstruction.

After applying all the selections described above, the distribution of the events in x_γ^{meas} is as shown in fig. 3. A 80:20 mixture of direct:resolved RAPGAP events gives a reasonable description of the data and was used subsequently. The event weighting described below was applied to the RAPGAP events plotted here. To evaluate the acceptances, allowance must be made for the different acceptances for the direct and the resolved processes, as modelled by PYTHIA and using the 80:20 mixture of RAPGAP-simulated direct and resolved events, each component previously normalised to the data.

From Fig. 4, in which all the above selections were applied except that on η^{max}, it can be seen that the distribution of the events in η^{max} is not well described by RAPGAP, normalised to the data. To compensate for this in calculating the acceptances, a weighting factor for events with $\eta^{\mathrm{max}} < 2.5$ was applied to the RAPGAP events. This does not have a large effect on the acceptances, since these do not vary greatly with η^{max}.

After applying all the selections described above with the exception of that on $x_{I\!P}$ the distribution of the events in $x_{I\!P}$ is as shown in fig. 5. The description in terms of weighted RAPGAP events, normalised to the data, is reasonable.

Two further corrections were applied to the HERA-II data, which were used to provide the results presented below. The total cross sections for the diffractive processes were evaluated at the detector level, and the HERA-II data were rescaled to have the same total cross section as measured using the HERA-I data. This compensated for a potential loss of events in the HERA-II data due to scattering of forward-generated particles off a beamline magnet that occupied most of the central aperture of the forward ZEUS calorimeter in the HERA-II running, but which was absent during the HERA-I running. The HERA-I Forward Proton Calorimeter removed additional non-diffractive events in this angular region..

A second correction was needed to remove non-diffractive events that succeeded in passing the diffractive event selections described above. This correction was evaluated using PYTHIA and HERWIG photoproduction event samples. These were normalised to the data sample after extracting the photon signal without applying the diffractive event selections. An appropriate mixture of resolved and direct photoproduction events was used. The diffractive event selections were then applied to the Monte Carlo samples to estimate the contribution of the photoproduction to the observed data, taking into account the contribution of the diffractive component to the photoproduction sample.

The mean of the two corrections was applied, and half the difference between them was taken as a systematic uncertainty.

7 Systematic uncertainties

The most significant sources of systematic uncertainty arose from the scaling of the HERA-II cross sections to the HERA-I data, treated as a systematic uncertainty although its origin is statistical. This amounts to an uncertainty of ±20%. The next most significant source comes from the uncertainty in the non-diffractive correction and was typically ±10%.

Other than these, the most significant sources of systematic uncertainty were evaluated as follows:

- to allow for uncertainties in the simulation of the hadronic final state, the cross sections were recalculated using HERWIG to model the signal and background events. The ensuing changes in the results correspond to an uncertainty of typically up to 8%, but rising to 18% in the highest bin of x_γ^{meas};
- the energy of the photon candidate was varied by ±2% in the MC at the detector level. Independently, the energy of the accompanying jet was varied by an amount decreasing from ±4.5% to ±2.5% as E_T^{jet} increases from 4 GeV to above 10 GeV. Each of these gave variations in the measured cross sections of typically 5%.

Further systematic uncertainties are as follows:

- the uncertainty in the acceptance due to the estimation of the relative fractions of direct and resolved events and radiative events in the MC sample was estimated by varying these fractions by ±15% and ±5% respectively in absolute terms; the changes in the cross sections were typically ±2% in each case;
- the dependence of the result on the modelling of the hadronic background by the MC was investigated by varying the upper limit for the $\langle \delta Z \rangle$ fit in the range $[0.6, 1.0]$; this gave a ±2% variation;
- the E_T^γ, η^{jet} and $\Delta\phi$ distributions in the MC were reweighted simultaneously to provide a closer agreement with the data, and the cross sections were re-evaluated. This generated changes of typically ±2%.

Other sources of systematic uncertainty were found to be negligible. These included the modelling of the track-isolation cut and the track-momentum cut, and also the cuts on photon isolation, the electromagnetic fraction of the photon shower, y_{JB} and Z_{vtx}. Except for the uncertainty on the modelling of the hadronic final state, the major uncertainties were treated as symmetric, and all the uncertainties were combined in quadrature. The uncertainties of 2.0% on the trigger efficiency and 1.9% on the luminosity measurement were not included in the figures.

8 Results

Differential cross sections were calculated for the production of an isolated photon, inclusive and with at least one accompanying jet, in the kinematic region defined by $Q^2 < 1$ GeV^2, $0.2 < y < 0.7$, $-0.7 < \eta^\gamma < 0.9$, $5 < E_T^\gamma < 15$ GeV, $4 < E_T^{\rm jet} < 35\,$GeVand $-1.5 < \eta^{\rm jet} < 1.8$. The diffractive condition consisted in requirements that $x_{I\!P} < 0.03$ amd $\eta^{\rm max} < 2.5$ at the hadron level.

All quantities were evaluated at the hadron level in the laboratory frame, and the jets were formed according to the k_T clustering algorithm with the radius parameter set to 1.0. Photon isolation was imposed such that at least 90% of the energy of the jet-like object containing the photon originated from the photon. If more than one accompanying jet was found within the designated $\eta^{\rm jet}$ range in an event, that with highest $E_T^{\rm jet}$ was taken. Cross sections in $E_T^{\rm jet}$ above 15 GeV are omitted from Fig. 9 owing to limited statistics, but this kinematic region is included in the other cross-section measurements.

Differential cross sections in the above kinematic region are presented for the quantities $E_T^\gamma, \eta^\gamma, E_T^{\rm jet}$ and $\eta^{\rm jet}$. The weighted predictions of Rapgap, normalised to the data, are also shown and are in reasonable agreement. Rapgap also gives a good description of the distributions in $x_\gamma^{\rm meas}$ and $x_{I\!P}$ (figs. 3,5).

For the quantity $z_{I\!P}^{\rm meas}$, the distributions of events are also shown and compared to Rapgap. In contrast to the dijet channel [14], the data show a sharp peak at the upper end of the distribution which is not described by Rapgap. One possible origin of events of this type could be from radiative DIS processes; this was studied using simulated events generated with the DJANGOH program interfaced with ARIADNE, and was estimated as contributing up to a level of 9 events for $z_{I\!P}^{\rm meas} > 0.90$ in the present analysis. The photoproduction background evaluated from Pythia and from Herwig is in both cases smooth in $z_{I\!P}^{\rm meas}$ up to unity.

The results here are inclusive of proton excitation processes which have been estimated to comprise approximately 16% of the total diffractive cross section.

9 Conclusions

The diffractive production of isolated photons with and without an accompanying jet has been measured in photoproduction with the ZEUS detector at HERA using an integrated luminosity of 374 ± 7 pb^{-1}. The present measurements extend earlier ZEUS results. Differential cross sections are presented in a kinematic region defined in the laboratory frame by: $Q^2 < 1$ GeV^2, $0.2 < y < 0.7$, $-0.7 < \eta^\gamma < 0.9$, $5 < E_T^\gamma < 15$ GeV, $4 < E_T^{\rm jet} < 35$ GeV and $-1.5 < \eta^{\rm jet} < 1.8$. A diffractive requirement was defined by the conditions $x_{I\!P} < 0.03$ and $\eta^{\rm max} < 2.5$. Photon isolation was imposed such that at least 90% of the energy of the jet-like object containing the photon originated from the photon.

Differential cross sections are given in terms of the transverse energy and pseudorapidity of the photon and of the jet. The shape of these distributions is satisfactorily described by the Rapgap Monte Carlo model, normalised to the data. The shapes of the distributions in $\eta^{\rm max}$ and $z_{I\!P}^{\rm meas}$ are not well described. In particular, a prominent peak near $z_{I\!P}^{\rm meas} = 1$ is seen and requires further study.

Acknowledgements

We appreciate the contributions to the construction, maintenance and operation of the ZEUS detector made by many people who are not listed as authors. The HERA machine group and the DESY computing staff are especially acknowledged for their success in providing excellent operation of the collider and the data-analysis environment. We thank the DESY directorate for their strong support and encouragement. We also thank H Jung for providing assistance with Rapgap..

References

[1] ZEUS Collaboration, H. Abramowicz et al., Phys. Lett. B 730 (2014) 293.

[2] ZEUS Collaboration, J. Breitweg et al., Phys. Lett. B 413 (1997) 201.

[3] ZEUS Collaboration, J. Breitweg et al., Phys. Lett. B 472 (2000) 175.

[4] ZEUS Collaboration, S. Chekanov et al., Phys. Lett. B 511 (2001) 19.

[5] ZEUS Collaboration, S. Chekanov et al., Eur. Phys. J. C 49 (2007) 511.

[6] H1 Collaboration, A. Aktas et al., Eur. Phys. J. C 38 (2004) 437.

[7] H1 Collaboration, F.D. Aaron et al., Eur. Phys. J. C 66 (2010) 17.

[8] H1 Collaboration, F.D. Aaron et al., Eur. Phys. J. C 54 (2008) 371.

[9] ZEUS Collaboration, S. Chekanov et al., Phys. Lett. B 595 (2004) 86.

[10] ZEUS Collaboration, S. Chekanov et al., Phys. Lett. B 687 (2010) 16.

[11] ZEUS Collaboration, H. Abramowicz et al., Phys. Lett. B 715 (2012) 88.

[12] ZEUS Collaboration, M. Derrick et al., Phys. Lett. B 384 (1996) 401.

[13] H1 Collaboration, C. Adloff et al., Eur. Phys. J. C 6 (1999) 421.

[14] ZEUS Collaboration, S. Chekanov et al., Eur. Phys. J. C 55 (2008) 171.

[15] H1 Collaboration, F. D. Aaron et al., Eur. Phys. J. C 70 (2008) 15.

[16] H1 Collaboration, V. Andreev et al., Phys. Lett. B 672 (2009) 219.

[17] ZEUS Collaboration, U. Holm (ed.), *The ZEUS Detector.* Status Report (unpublished), DESY (1993), available on `http://www-zeus.desy.de/bluebook/bluebook.html`.

[18] N. Harnew et al., Nucl. Inst. Meth. A 279 (1989) 290;
B. Foster et al., Nucl. Phys. Proc. Suppl. B 32 (1993) 181;
B. Foster et al., Nucl. Inst. Meth. A 338 (1994) 254.

[19] A. Polini et al., Nucl. Inst. Meth. A 581 (2007) 656.

[20] M. Derrick et al., Nucl. Inst. Meth. A 309 (1991) 77;
A. Andresen et al., Nucl. Inst. Meth. A 309 (1991) 101;
A. Caldwell et al., Nucl. Inst. Meth. A 321 (1992) 356;
A. Bernstein et al., Nucl. Inst. Meth. A 336 (1993) 23.

[21] L. Adamczyk et al., Nucl. Inst. Meth. A 744 (2014) 80.

[22] J. Andruszków et al., Preprint DESY-92-066, DESY, 1992;
ZEUS Collaboration, M. Derrick et al., Z. Phys. C 63 (1994) 391;
J. Andruszków et al., Acta Phys. Pol. B 32 (2001) 2025.

[23] M. Helbich et al., Nucl. Inst. Meth. A 565 (2006) 572.

[24] J. Pumplin et al., JHEP 02 (2006) 032.

[25] M.A. Kimber, A.D. Martin and M.G. Ryskin, Phys. Rev. D 63 (2001) 114027; G. Watt, A.D. Martin and M.G. Ryskin, Eur. Phys. J. C 31 (2003) 73.

[26] A.D. Martin et al., Eur. Phys. J. C 63 (2009) 189.

[27] T. Sjöstrand et al., JHEP 05 (2006) 26.

[28] H.L. Lai et al., Phys. Rev. D 55 (1997) 1280.

[29] M. Glück, G. Reya and A. Vogt, Phys. Rev. D 45 (1992) 3986; M. Glück, G. Reya and A. Vogt, Phys. Rev. D 46 (1992) 1973.

[30] G. Corcella et al., JHEP 01 (2001) 010.

[31] R. Brun et al., GEANT3, Technical Report CERN-DD/EE/84-1, CERN, 1987.

[32] W.H. Smith, K. Tokushuku and L.W. Wiggers, *Proc. Computing in High-Energy Physics (CHEP), Annecy, France, Sept. 1992*, C. Verkerk and W. Wojcik (eds.), p. 222. CERN, Geneva, Switzerland (1992). Also in preprint DESY 92-150B.

[33] P. Allfrey et al., Nucl. Inst. Meth. A 580 (2007) 1257.

[34] ZEUS Collaboration, M. Derrick et al., Phys. Lett. B 303 (1993) 183.

[35] ZEUS Collaboration, J. Breitweg et al., Eur. Phys. J. C 1 (1998) 81; ZEUS Collaboration, J. Breitweg et al., Eur. Phys. J. C 6 (1999) 43.

[36] S. Catani et al., Nucl. Phys. B 406 (1993) 187.

[37] S.D. Ellis and D.E. Soper, Phys. Rev. D 48 (1993) 3160.

[38] ZEUS Collaboration, S. Chekanov et al., Nucl. Phys. B 729 (2005) 492; ZEUS Collaboration, S. Chekanov et al., Phys. Rev. D 76 (2007) 072011; ATLAS Collaboration, G. Aad et al., Nucl. Phys. B 875 (2013) 483.

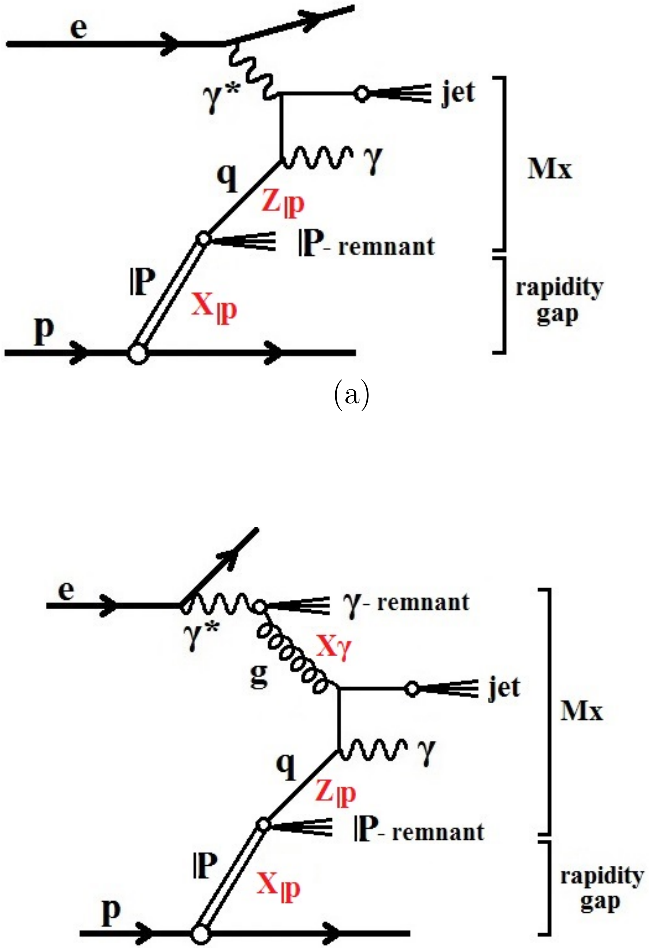

Figure 1: *Examples of the diffractive production of a prompt photon and a jet in ep scattering from (a) direct (b) resolved photons.*

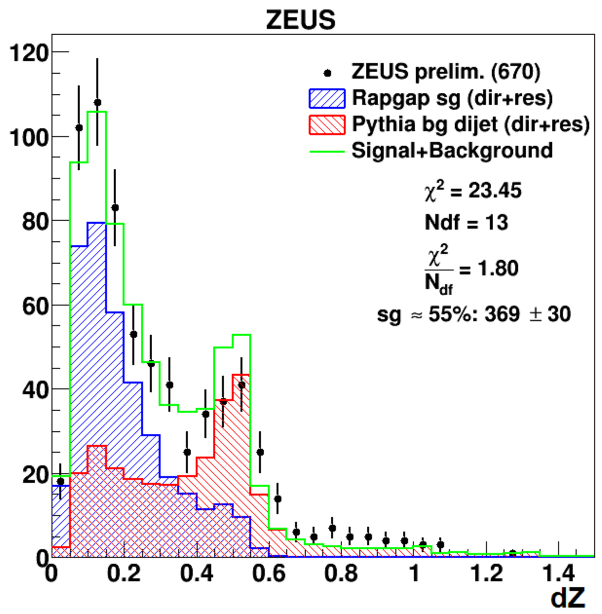

Figure 2: *Distribution of* $\langle \delta Z \rangle$ *for diffractive events, The error bars denote the statistical uncertainties on the data.*

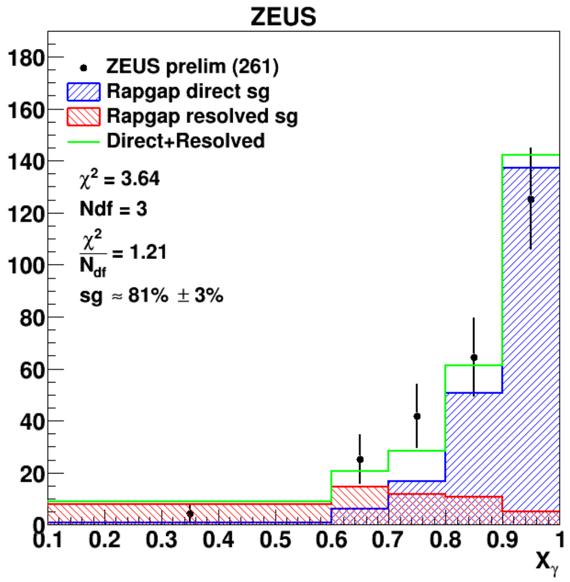

Figure 3: *Photon events detected as a function of* $x_\gamma^{\rm meas}$*, per unit interval of 0.1 in* $x_\gamma^{\rm meas}$*, and compared to a mixture of* RAPGAP*-generated direct and resolved events using the model described in the text. The simulated events were passed through the detector simulation and the kinematic selections described in the text were applied. No acceptance corrections were applied at this stage.*

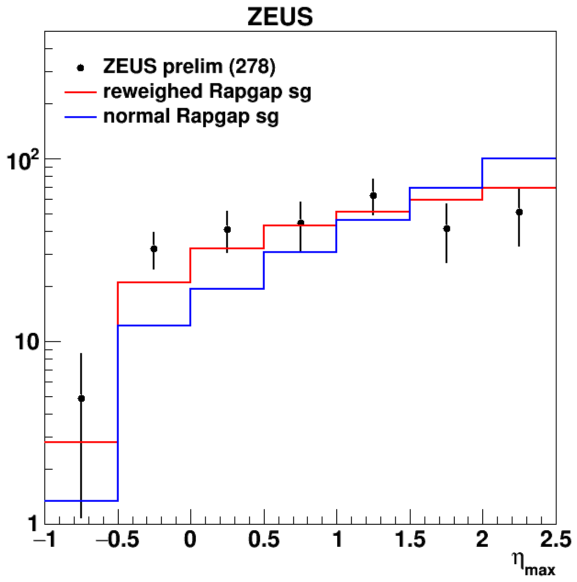

Figure 4: *Photon events detected as a function of* $\eta^{\max}$*, compared to a mixture of* Rapgap*-generated direct and resolved events, using the direct:resolved model described in the text. The simulated events were passed through the detector simulation and the kinematic selections described in the text were applied. No acceptance corrections were applied at this stage.*

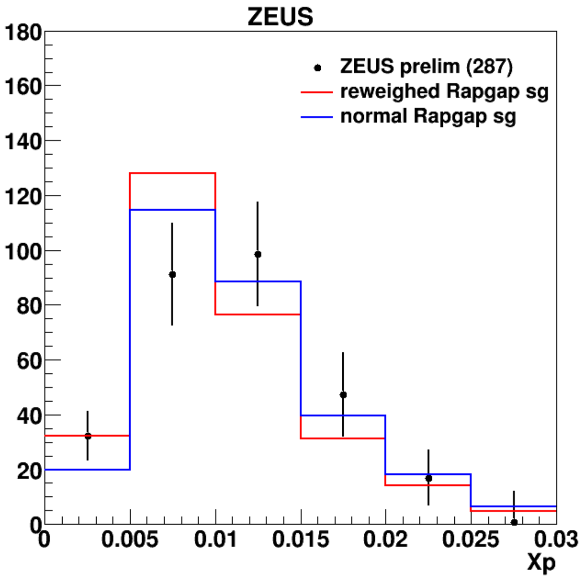

Figure 5: *Photon events detected as a function of* $x_{I\!P}$*, compared to a mixture of* Rapgap*-generated direct and resolved events using the direct:resolved model described in the text. The simulated events were passed through the detector simulation and the kinematic selections described in the text were applied. No acceptance corrections were applied at this stage.*

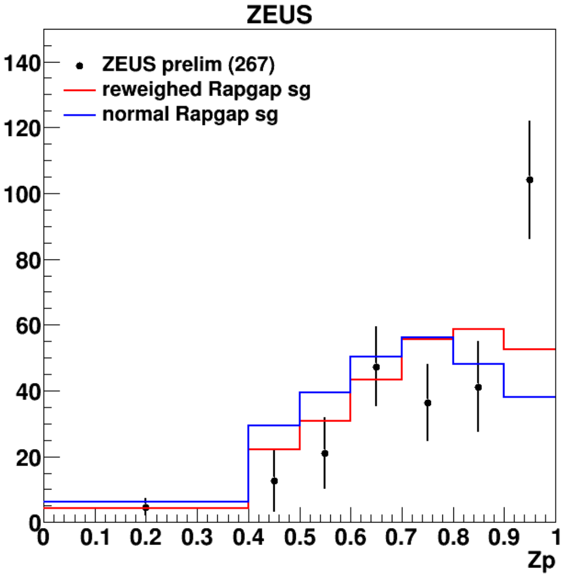

Figure 6: *Photon events detected as a function of* $z_{I\!P}^{\mathrm{meas}}$*, compared to a mixture of* Rapgap*-generated direct and resolved events using the direct:resolved model described in the text. The simulated events were passed through the detector simulation and the kinematic selections described in the text were applied. No acceptance corrections were applied at this stage.*

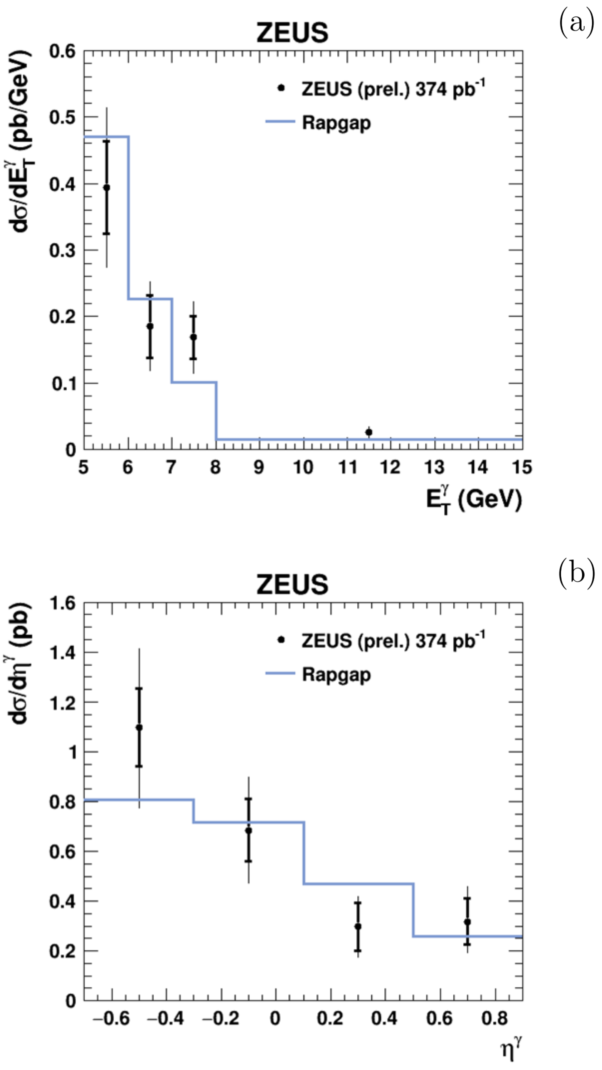

Figure 7: *Differential cross sections as functions of (a) E_T^γ and (b) η^γ, for events containing an isolated photon, compared to normalised prediction from* Rapgap.. *The kinematic region of the measurement is described in the text. The inner and outer error bars respectively denote statistical uncertainties and statistical with systematic uncertainties combined in quadrature..*

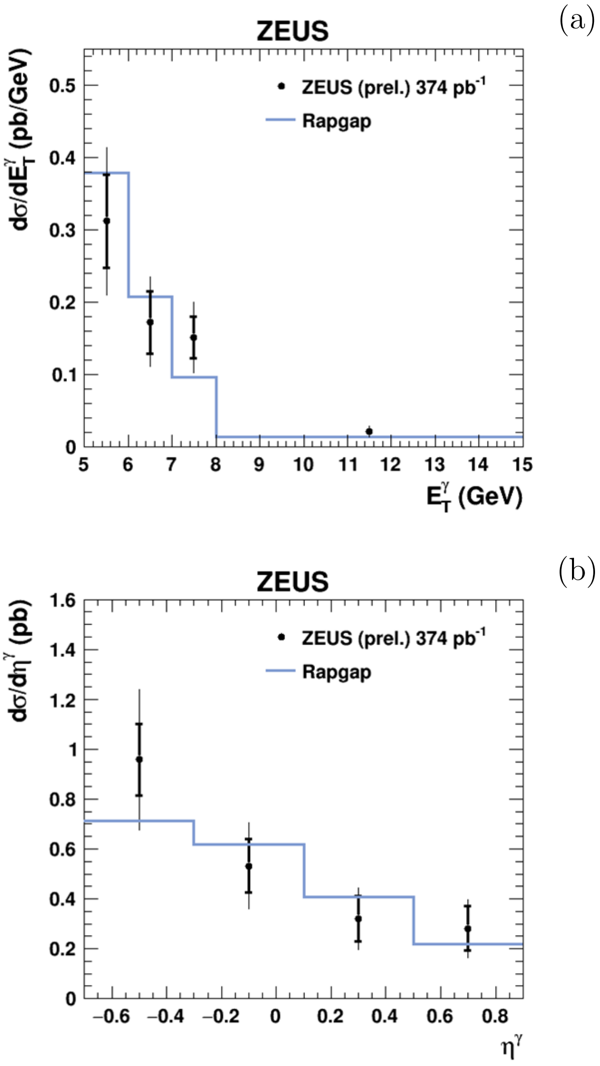

Figure 8: *Differential cross sections as functions of (a) E_T^γ and (b) η^γ, for events containing an isolated photon accompanied by a jet, compared to normalised prediction from* Rapgap.*. The kinematic region of the measurement is described in the text. The inner and outer error bars respectively denote statistical uncertainties and statistical with systematic uncertainties combined in quadrature..*

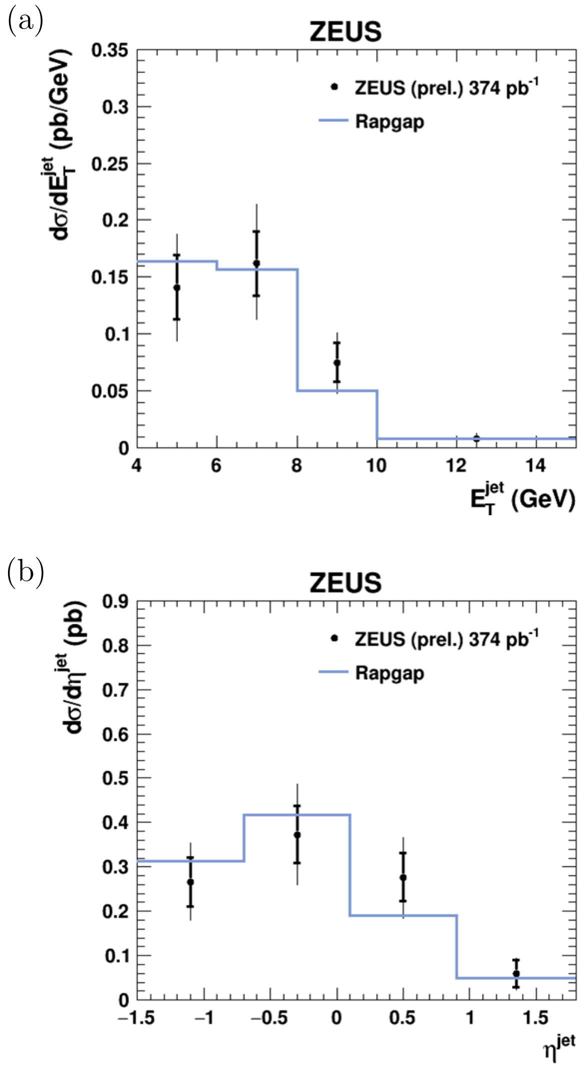

Figure 9: *Differential cross sections as functions of (a) E_T^{jet} and (b) η^{jet}, for events containing an isolated photon accompanied by a jet, compared to normlised prediction from* Rapgap. *The kinematic region of the measurement is described in the text. The inner and outer error bars respectively denote statistical uncertainties and statistical uncertainties with systematic uncertainties combined in quadrature.*

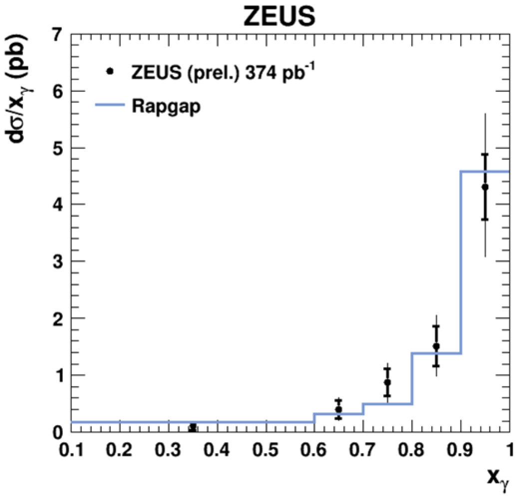

Figure 10: *Differential cross section as a function of x_γ^{meas}, for events containing an isolated photon and a jet, compared to normlised prediction from* Rapgap. *The kinematic region of the measurement is described in the text. The inner and outer error bars respectively denote statistical uncertainties and statistical uncertainties combined with systematic uncertainties in quadrature. hatched and dotted bands.*

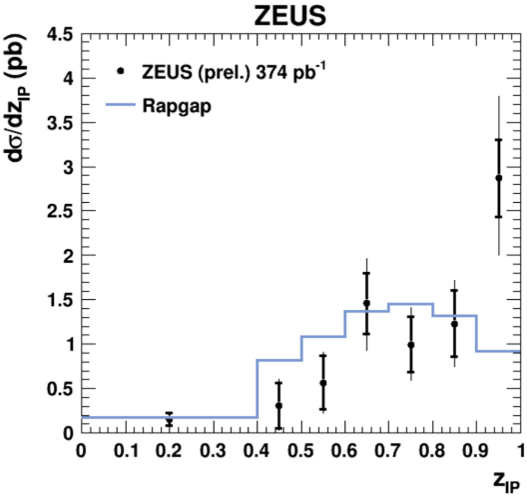

Figure 11: *Differential cross section as a function of $z_{I\!P}^{\text{meas}}$, for events containing an isolated photon and a jet, compared to normlised prediction from* Rapgap. *The kinematic region of the measurement is described in the text. The inner and outer error bars respectively denote statistical uncertainties and statistical uncertainties combined with systematic uncertainties in quadrature. hatched and dotted bands.*